JACS
JOURNAL OF THE AMERICAN CHEMICAL SOCIETY
Article
pubs.acs.org/JACS

Transition State Analysis of Acid-Catalyzed Hydrolysis of an Enol Ether, Enolpyruvylshikimate 3-Phosphate (EPSP)

Meiyan Lou,[†] Meghann E. Gilpin,[§,†] Steven K. Burger,[‡] Ayesha M. Malik,[†] Vivian Gawuga,[‡] Vladimir Popović,[‡] Alfredo Capretta,[‡] and Paul J. Berti*[,‡,†]

[‡]Department of Chemistry & Chemical Biology, and [†]Department of Biochemistry & Biomedical Sciences, McMaster University, 1280 Main Street West, Hamilton, Ontario L8S 4M1, Canada

Ⓦ *Web-Enhanced Feature* Ⓢ *Supporting Information*

ABSTRACT: Proton transfer to carbon represents a significant catalytic challenge because of the large intrinsic energetic barrier and the frequently unfavorable thermodynamics. Multiple kinetic isotope effects (KIEs) were measured for acid-catalyzed hydrolysis of the enol ether functionality of enolpyruvylshikimate 3-phosphate (EPSP) as a nonenzymatic analog of the EPSP synthase (AroA) reaction. The large solvent deuterium KIE demonstrated that protonating C3 was the rate-limiting step, and the lack of solvent hydron exchange into EPSP demonstrated that protonation was irreversible. The reaction mechanism was stepwise, with C3, the methylene carbon, being protonated to form a discrete oxacarbenium ion intermediate before water attack at the cationic center, that is, an $A_H^{\ddagger}{}^*A_N$ (or $A_H^{\ddagger} + A_N$) mechanism. The calculated 3-^{14}C and 3,3-$^2H_2$ KIEs varied as a function of the extent of proton transfer at the transition state, as reflected in the C3−H$^+$ bond order, n_{C3-H+}. The calculated 3-^{14}C KIE was a function primarily of C3 coupling with the movement of the transferring proton, as reflected in the reaction coordinate contribution ($^{light}\nu^{\ddagger}/^{heavy}\nu^{\ddagger}$), rather than of changes in bonding. Coupling was strongest in early and late transition states, where the reaction coordinate frequency was lower. The other calculated ^{14}C and ^{18}O KIEs were more sensitive to interactions with counterions and solvation in the model structures than n_{C3-H+}. The KIEs revealed a moderately late transition state with significant oxacarbenium ion character and with a C3−H$^+$ bond order ≈0.6.

INTRODUCTION

Protonation and deprotonation of carbon bases and acids represents a significant challenge to both enzymatic and nonbiological catalysts. There is a large intrinsic barrier not encountered in proton transfer between electronegative atoms, and the free energies of forming carbon-centered cations or anions are frequently unfavorable.[1] Proton transfer to and from carbon atoms represents a major catalytic challenge for important classes of enzymatic reactions, including terpene cyclases,[2] enolases,[3] and epimerases/racemases.[4] The most difficult catalytic step—the catalytic imperative—for the carboxyvinyl transferases AroA (EPSP synthase)[5−11] and MurA[12] is protonating the methylene carbon of an enol ether functionality.

Enol ether protonation is general acid-catalyzed, and increased free energy of protonation tends to correlate with later transition states (TSs), i.e., with greater bond order to the carbon base, as expected from the Hammond postulate.[13−15] It also tends to correlate with smaller primary deuterium kinetic isotope effects (KIEs). The reaction is catalyzed by carboxylic acids in preference to H_3O^+, even at modest buffer concentrations.[16−18] The position of the transition state can by roughly estimated from the Brønsted exponent values, α. For many carboxylic acid-catalyzed vinyl ether hydrolyses, α = 0.6−0.7,[16,17,19,20] though it is slightly lower for positively charged amino acids such as glycine.[16] This can be taken as a rough measure of the extent of bond formation to the carbon acid, though there is evidence that α overestimates the extent of proton transfer by at least 0.1.[21] Thus, based on α values, the transition states would be expected to be roughly balanced (i.e., bond orders from the general acid to the transferring proton and the transferring proton to the carbon base are equal) or slightly late. Recent experimental and computational studies on enol ether hydrolysis have focused on product isotope effects (PIEs) of α-methoxystyrenes.[18,22,23] The PIEs on this homologous series of reactants revealed that there was no quantum tunneling during proton transfer and that the transition state was roughly balanced.[18,22] A computational study of the primary deuterium KIEs on the same compounds supported the conclusion that tunneling was a minor factor in lowering the free energy barriers to reaction, though tunneling corrections were needed for the best accuracy in KIE calculations.[23] It also showed that the extent of proton transfer in computational TS structures was strongly dependent on the free energy of the reaction, showing a Hammond shift as expected; that is, less favorable reactions had later transition states.

In order to better understand AroA catalysis, we have performed TS analysis on the acid-catalyzed hydrolysis of

Received: May 4, 2012
Published: July 5, 2012

dx.doi.org/10.1021/ja3043382 | J. Am. Chem. Soc. 2012, 134, 12947−12957

Scheme 1

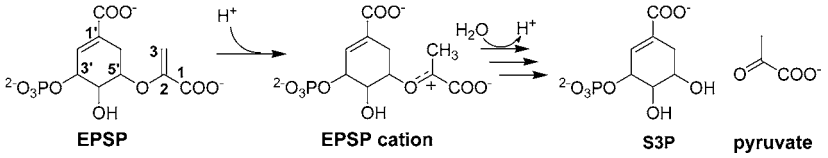

enolpyruvylshikimate 3-phosphate (EPSP) as an analog of the enzymatic reaction. In the AroA-catalyzed reaction the catalytic imperative is protonating the methylene carbon of phosphoenolpyruvate (PEP), or EPSP in the reverse reaction.[6−11] The EPSP cation then undergoes nucleophilic addition by phosphate (P_i), to form a tetrahedral intermediate (THI), and ultimately shikimate 3-phosphate (S3P) and PEP. Likewise, the catalytic imperative for acid-catalyzed hydrolysis is protonating the methylene carbon (Scheme 1). Understanding the nonenzymatic mechanism helps illuminate catalysis, as enzymatic catalysis reflects an interplay between a substrate's intrinsic reactivity and catalytic strategies to lower the activation energy.

In this study, we used multiple KIEs to determine the TS structure.[24−26] KIEs are the most direct and detailed experimental approach to TS structure determination. Each KIE consists of a "structural contribution" and a "reaction coordinate contribution", also called the temperature independent factor.[27] The reaction coordinate contribution arises from the normal vibrational mode with an imaginary frequency (sometimes written as a negative frequency) which describes atoms' movements through the transition state from reactants to products. Its contribution to the KIE is the ratio of reaction coordinate frequencies, $^{light}\nu^{\ddagger}/^{heavy}\nu^{\ddagger}$, and it is ≥ 1.[27,28] It can be separated numerically from the "structural contribution", which reflects changes in bond strengths. A bond becoming weaker at the transition state will give a normal structural contribution, i.e., $^{light}k/^{heavy}k > 1$. If the bond becomes stronger, the structural contribution will be inverse, i.e., $^{light}k/^{heavy}k < 1$. The structural contribution is generally dominated by the zero point energy (ZPE) term, with further contributions from vibrationally excited states (EXC) and the change in mass and moments of inertia, as reflected in the vibrational product (VP).[29] The structural contribution is temperature dependent and is given by ZPE × EXC × VP. The overall KIE is KIE = $(^{light}\nu^{\ddagger}/^{heavy}\nu^{\ddagger})$(ZPE × EXC × VP).[28,30] If a tunneling correction is used, it is included as a separate term, e.g., Q_{Bell}.[31,32]

In this study we describe the TS analysis of acid-catalyzed EPSP hydrolysis, while the accompanying publication describes AroA-catalyzed EPSP hydrolysis.[33]

MATERIALS AND METHODS

General. All reagents were purchased from Sigma-Aldrich or Bioshop Canada (Burlington, ON), except as noted. [1-^{14}C]Pyruvate was from GE Healthcare; [2-^{14}C]- and [3-^{14}C]pyruvate were from American Radiolabeled Chemicals (St. Louis, MO). [γ-^{33}P]- and [γ-^{32}P]ATP were from Perkin-Elmer, and ^2H_2O was from Cambridge Isotope Laboratories. His-tagged *E. coli* AroA was prepared and assayed as described previously.[7,10] S3P was prepared as described previously.[10]

ppsA. A plasmid for expressing phosphoenolpyruvate synthetase (ppsA) was a gift from Dr. David Jakeman (Dalhousie University). ppsA was overexpressed as described previously[34] and partially purified. Cell debris from ammonium sulfate at 40% saturation was removed by centrifugation, at 11,000*g* for 15 min, then ammonium sulfate was increased to 50% saturation, and the precipitated ppsA was collected by centrifugation. It was redissolved in 50 mM Tris·Cl, pH 6.8, 1 mM DTT, and 1.5 mM NaN_3. The protein concentration was determined with the Bradford assay.[35]

EPSP Synthesis. Unlabeled EPSP was synthesized using 1 μM AroA, 1 mM S3P, and 2 mM PEP in 50 mM K·HEPES, pH 7.0, with overnight incubation at 37 °C, and purified as described previously.[8]

Radiolabeled EPSP. [1-^{14}C]-, [2-^{14}C]-, and [3-^{14}C]EPSP were synthesized from S3P and [1-^{14}C]-, [2-^{14}C]-, or [3-^{14}C]pyruvate using ppsA and AroA (Scheme 2). The reactions contained 10 mM pyruvate

Scheme 2

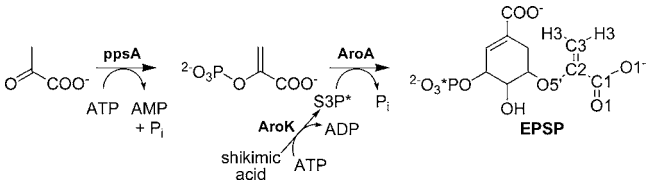

(10 μCi ^{14}C), 12 mM S3P, 15 mM ATP, 15 mg/mL ppsA, and 1 μM AroA in 50 mM Tris·Cl, pH 7.5, 5 mM KCl, and 10 mM $MgCl_2$, with the pH adjusted to ≈7.5 with KOH before the enzymes were added and incubated at 37 °C overnight. Reactions typically reached ≈80% completion.

[^{32}P]- and [^{33}P]EPSP were synthesized from shikimic acid and [γ-^{32}P]- or [γ-^{33}P]ATP using shikimate kinase[36] (AroK) and AroA (Scheme 2). Reactions contained 0.7 mM shikimic acid, 0.7 mM PEP, 0.15 mM [γ-^{32}P]- or [γ-^{33}P]ATP (25 μCi), 70 nM AroA, and 7 μL/mL AroK in 50 mM Tris·Cl, pH 7.5, 3 mM KCl, 0.7 mM $MgCl_2$, and 2 mM sodium tungstate, with the pH adjusted to ≥7.5 with KOH before the enzymes were added. Low reactant concentrations were used to avoid ADP product inhibition. Reactions typically reached ≈70% completion after overnight incubation at 37 °C.

[^{33}P,5′-^{18}O]EPSP synthesis was the same as [^{33}P]EPSP, except using [5-^{18}O]shikimic acid, which was synthesized as described previously.[37] A reaction with nonradioactive ATP was run in parallel, and mass spectrometry was used to determine that the ^{18}O enrichment was 55%. The observed KIEs were corrected for the extent of labeling.

[^{33}P,3,3-$^2H_2$]EPSP was synthesized from [^{33}P]EPSP by equilibrating it in D_2O with 1 μM AroA and 5 mM potassium phosphate, pD 7.5, at 37 °C. One solvent deuteron is incorporated in each catalytic cycle. Allowing the reaction to equilibrate overnight resulted in quantitative EPSP deuteration. Mass spectrometry of a parallel reaction using unlabeled EPSP showed 97% ^{2}H incorporation.

[^{33}P,1,1-$^{18}O_2$]EPSP was synthesized from [^{33}P]S3P and [$^{18}O_5$]PEP. [^{33}P]S3P was synthesized using 20 mM shikimic acid, 10 mM PEP, 2 mM [γ-^{33}P]ATP (25 μCi), 100 μL/mL of partially purified AroK, and 60 U/mL pyruvate kinase in 50 mM Tris·Cl, pH 7.5, 50 mM KCl, 10 mM $MgCl_2$, and 25 mM sodium tungstate. [^{33}P]S3P was purified under the same conditions as EPSP,[8] and solvent was removed by lyophilization. [$^{18}O_5$]PEP was synthesized by oxygen atom exchange of 90 mM PEP in $H_2{}^{18}O$, catalyzed by 1.5 M H_2SO_4 at 95 °C for 30 min, and then neutralized with KOH. [$^{18}O_5$]PEP was reacted with [^{33}P]S3P to produce [^{33}P,1,1-$^{18}O_2$]EPSP, as described above. Mass spectrometry of parallel reactions using unlabeled S3P showed 83−91% ^{18}O incorporation in different reactions. KIEs were corrected for the extent of labeling.

EPSP Hydrolysis. Acid-catalyzed EPSP hydrolysis was performed with 500 μM EPSP in 50 mM ammonium acetate, pH 5.4, at 90 °C. The extent of EPSP hydrolysis was measured by anion exchange

dx.doi.org/10.1021/ja3043382 | J. Am. Chem. Soc. 2012, 134, 12947−12957

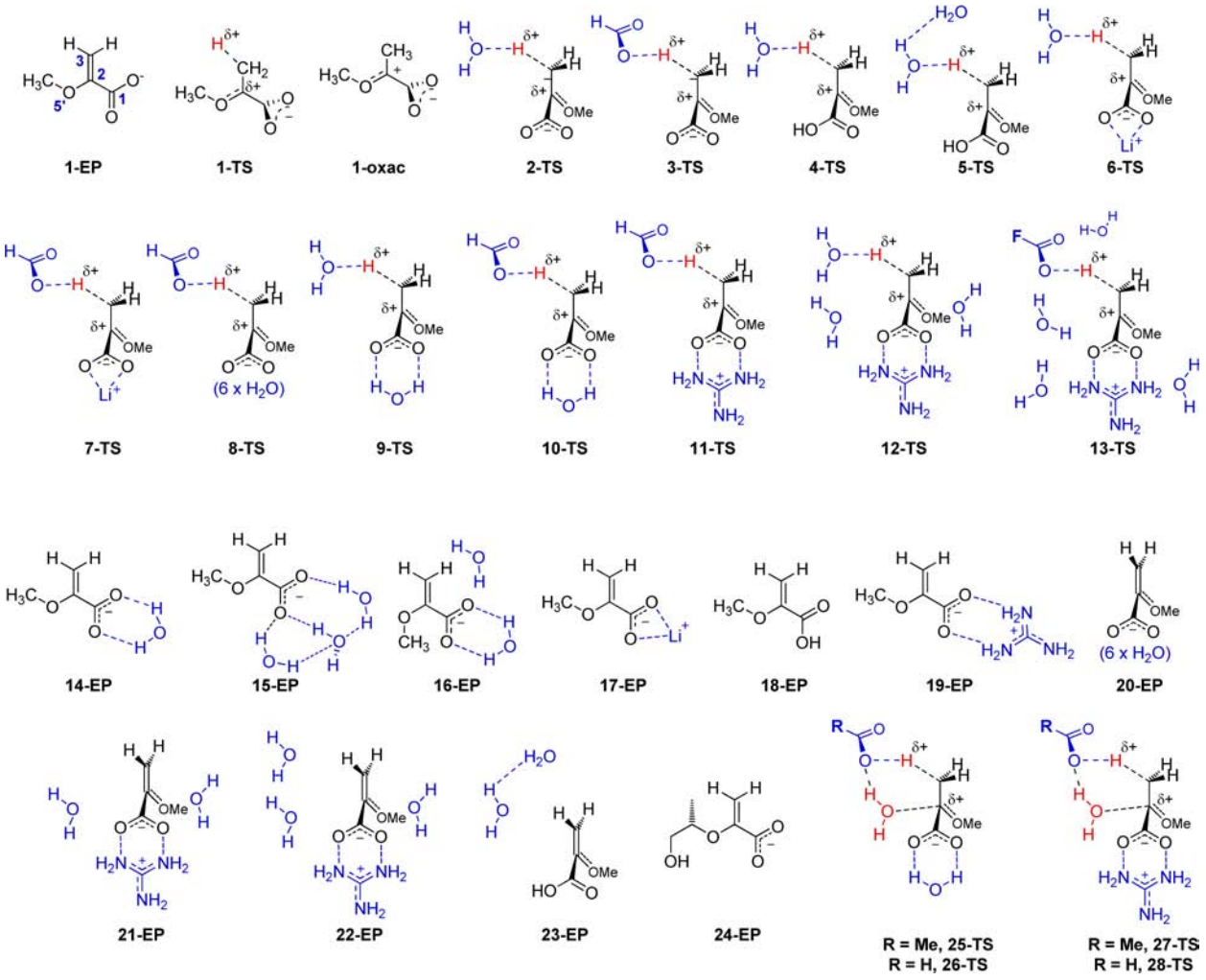

Figure 1. Computational models for IE calculations. Compound **1** is a generic model, with the suffix indicating the reactant (**EP**), transition state (**TS**), or oxacarbenium ion (**oxac**). For compounds **2**–**13**, only the **TS** models for C3 protonation are shown, though the corresponding **EP** structures and those **oxac** structures which were stable were also optimized (Tables S1–S4). For compounds **14**–**24**, **EP** and some **oxac** structures were optimized. When used in the text and tables, the suffix **scrf** indicates continuum solvation (see Material and Methods). Solvating waters in compound **13** were calculated at a lower level of theory using ONIOM methodology (see Material and Methods). Compounds **25**–**28** were for concerted protonation and water addition, i.e., an A_NA_H mechanism. Cartesian coordinates for structures in this figure appear in the Supporting Information (Table S5).

chromatography (Mono Q, 5 mm × 50 mm, GE Healthcare) of a 150 μL reaction aliquot under the same conditions as EPSP purification, using the ε_{240} ratio for S3P/PEP/EPSP of 0.59:1.0:2.1.[9] The hydrolytic rate constant, k_{hyd}, was then calculated.

Solvent Deuterium KIEs (SDKIEs). In order to avoid complications from isotope effects on the pK_a values of EPSP's ionizable groups, the acid-catalyzed SDKIE was determined at pL 2, in a plateau region of the pH profile.[8] Reactions contained 500 μM EPSP in 50 mM glycine, pL 2.0 at 52 °C, using the same HPLC assay as above.

Solvent Proton Incorporation. Solvent proton incorporation was monitored to test whether C3 protonation was the first irreversible step in EPSP hydrolysis. Solvent ^{1}H incorporation into [3,3-$^2H_2$]EPSP was monitored because the large SDKIE = 6.7 (see Results) would have biased the reaction against detecting ^{2}H incorporation into unlabeled EPSP. [3,3-$^2H_2$]EPSP (5 mM) in 50 mM glycine, pH 2.0, was reacted for 60 min at 52 °C. Negative-ion electrospray ionization mass spectra (ESI-MS) of residual EPSP were used to detect hydron exchange. Reaction aliquots (5 μL) were diluted into 500 μL of 50:48:2 MeOH/H_2O/formic acid, and mass spectra were collected. [3,3-$^2H_2$]EPSP gave m/z = 325, while one or two ^{1}H exchanges produced m/z = 324 or 323 peaks, respectively. The fractional extent of ^{1}H incorporation, $f(^1H)$, was calculated as follows:

$$f(^1H) = \frac{(2I_{323} + I_{324})}{2(I_{323} + I_{324} + I_{325})} \quad (1)$$

where I_n represents the integration of each EPSP peak in the mass spectrum. After correcting for the m/z = 324 ion at t = 0 due to incomplete labeling, the rate of ^{1}H incorporation (k_{ex}) was fitted to a first order rate equation.

Competitive KIE Measurement. Competitive KIEs were determined by measuring the change in isotope ratios between unreacted EPSP (0% reaction) and residual EPSP at ~50% reaction. For ^{14}C KIEs, ^{32}P was used as a reporter on ^{12}C at the position of interest, and the ratio r_i = ^{32}P/^{14}C was measured. For ^{2}H and ^{18}O KIEs, ^{33}P reported on the isotope of interest, and ^{32}P reported on ^{1}H or ^{16}O. In that case, r_i = ^{32}P/^{33}P. The higher energy β-particles emitted by ^{32}P can be distinguished from ^{33}P and ^{14}C by liquid scintillation counting.[38]

EPSP (0.25 μCi of each radiolabel) was repurified by C18 reverse phase HPLC (3.9 mm × 150 mm column) using isocratic elution in 50 mM ammonium acetate, pH 6, 44 mM KCl, and 2.5 mM tetrabutylammonium sulfate (TBAS), and a flow rate of 1 mL/min.

dx.doi.org/10.1021/ja3043382 | J. Am. Chem. Soc. 2012, 134, 12947–12957

The ~2 mL fraction containing EPSP was adjusted to pH 5.40 ± 0.03 with HCl. One-third of the volume was taken as the unreacted sample (0% reaction), while the rest was incubated at 90 °C for 50 min to reach ~50% completion. The 0% and 50% samples were injected separately on a Mono Q anion exchange column and eluted with a gradient of 100−500 mM KCl in 10 mM NH_4Cl, pH 10.0, at 0.5 mL/min over 26 min. The complete peaks of pyruvate (4−11 min), S3P (11−16 min), EPSP ketal (16−18 min),[8] and EPSP (18−26 min) were collected. The liquid weight of each fraction was adjusted to equal that of the EPSP peak using buffer with the same composition as where EPSP eluted, i.e., 300 mM KCl, 10 mM NH_4Cl, pH 10.0. Each peak was split equally into two scintillation vials and neutralized with 100 μL of 0.5 M potassium phosphate, pH 6.0, before 20 mL of Liquiscint (National Diagnostics) was added. A blank and a ^{32}P standard were prepared with an appropriate weight of elution buffer. Each vial was counted for 10 min repeatedly, until the 95% confidence interval of the observed KIE was <0.005.

The extent of reaction, f, was calculated using eq 2:

$$f = (\mathrm{cpm}_{\mathrm{pyruvate}} + \mathrm{cpm}_{\mathrm{S3P}} + \mathrm{cpm}_{\mathrm{ketal}}) / (\mathrm{cpm}_{\mathrm{pyruvate}} + \mathrm{cpm}_{\mathrm{S3P}} + \mathrm{cpm}_{\mathrm{ketal}} + \mathrm{cpm}_{\mathrm{EPSP}}) \quad (2)$$

where cpm_x is the radioactivity from all radionuclides in the chromatographic peak for each species. KIEs were calculated from the isotope ratios, r_i, in EPSP at 0% and 50% reaction using eq 3:[39]

$$\mathrm{KIE} = \frac{\ln\left[\frac{(1-f)(1+r_0^{-1})}{(1+r_f^{-1})}\right]}{\ln\left[\frac{(1-f)(1+r_0)}{(1+r_f)}\right]} \quad (3)$$

where r_0 and r_f are the isotope ratios at the beginning and at extent f of the reaction, respectively.

In control experiments, complete radioisotope chromatograms of ^{14}C- and ^{32}P-containing reaction mixtures at 0% and 50% reaction were collected in 250 μL fractions to confirm that only the expected products were observed. The effect of chromatography on the isotope ratio, r_i, was also checked. A mixture of [^{14}C]- and [^{32}P]EPSP was repurified as above. The entire EPSP peak was collected, and half (#1) was diluted into 20 mL of scintillation fluid while the other half (#2) was rechromatographed again and the EPSP peak collected again. The isotope ratios, r_i, were measured in each sample and found to be equal; $r_{\#1}/r_{\#2} = 0.998 \pm 0.003$.

Electronic Structure Calculations. KIEs and EIEs were calculated from quantum mechanically optimized structures based on a generic methylenolpyruvate (**1**) model (see Figure 1). For compounds **1**−**13**, the reactant, transition state, and oxacarbenium ion structures were optimized wherever possible, though some structures (e.g., **1-oxac**) were not computationally stable. For compounds **14**−**24**, only reactant and oxacarbenium ion models were optimized. Compounds **25**−**28** were models of concerted protonation and water addition.

Quantum mechanical calculations were performed using hybrid density functional theory (DFT) with Becke's exchange functional,[40] Perdew and Wang's correlation functional,[41] and a 6-31+G** basis set (B3PW91/6-31+G**) with Gaussian 03 or 09.[42]

Solvent effects were modeled in some structures with a conductor-like polarizable continuum model (CPCM),[43] using a dielectric constant equal to water's, and UA0 atomic radii. An extra sphere was placed on the proton being transferred, and SCRF frequency calculations used numerical differentiation.[44] The ONIOM approach was used for some explicit solvating waters, modeled at the RHF/3-21+G level of theory.[45] The diffuse function, "+", prevented the water molecules from attacking C2 of the transition state and oxacarbenium ion models. Frequency calculations were done to ensure that optimized structures had no imaginary frequencies and TS structures had one, except as noted below.

The calculated IEs and structures were tested for sensitivity to the computational method using the MP2/aug-cc-pVDZ level of theory, i.e., second-order Møller−Plesset theory with Dunning's correlation consistent aug-cc-pVDZ basis set, and PBE0/aug-cc-pVDZ, i.e., the Perdew−Burke−Ernzerhof generalized gradient approximation DFT method. These methods were used for the **17-EP**/**6-TS** pair and the **14-EP**/**10-TS** pair (see Figure 1).

Stepwise (A_H*A_N or A_H + A_N) Transition States. Most TS structures were found by standard TS optimizations using the QST3 keyword.[46]

Structure **11-TS** did not fully converge. Multiple TS optimizations from different starting points converged toward a unique structure, but displacements in the solvating guanidinium molecule remained too large. An imaginary frequency of 11i cm^{-1} corresponding to rotation of guanidinium and the C1 carboxyl was below the normal 50i cm^{-1} cutoff for QUIVER (see below) and, therefore, neglected. The same problems were encountered with **11-TS-scrf** and **10-TS-scrf**. The H^+−OA and C3−H^+ bond lengths of these structures were scanned in 0.005 Å steps until a saddle point with a single imaginary frequency was found.

Concerted A_NA_H Transition States. Conventional optimizations failed to find any transition states for concerted water addition; rather, it was necessary to use a search scheme based on a reduced potential energy surface.[47] An initial guess of the transition state was generated using a one-dimensional scan with the H^+−OA distance; then, the Bofill update TS searching scheme confined to a two-dimensional reduced potential energy surface was used (see ref 47). The two coordinates used were the H^+−OA and C3−H^+ distances. Each step of the procedure required a constrained minimization using the MODRED keyword in Gaussian. When the optimization was converged, an additional TS optimization was performed using the OPT(EIGENTEST,CALCALL) keywords to ensure that the system had only one imaginary frequency.

EIE and KIE Calculation. QUIVER[48] was used to calculate reduced isotopic partition functions (Q) at 363 K. The Cartesian force constants were scaled by 0.9139 (= 0.956^2).[49] Equilibrium isotope effects (EIEs) were calculated using eq 4:

$$\mathrm{EIE} = Q_{\mathrm{initial}}/Q_{\mathrm{final}} \quad (4)$$

and KIEs were calculated using eq 5:

$$\mathrm{KIE} = Q_{\mathrm{initial}}/Q^{\ddagger} \times {}^{\mathrm{light}}\nu^{\ddagger}/{}^{\mathrm{heavy}}\nu^{\ddagger} \times Q_{\mathrm{Bell}} \quad (5)$$

where $Q^{\ddagger}$ is the partition function calculated with the $3N - 7$ normal modes of the transition state, ${}^{\mathrm{light}}\nu^{\ddagger}$ and ${}^{\mathrm{heavy}}\nu^{\ddagger}$ are the imaginary frequencies, and Q_{Bell} is the Bell tunneling correction (eq 6):[31,32]

$$Q_{\mathrm{Bell}} = \frac{|{}^{\mathrm{light}}u^{\ddagger}|/2 \,/\, \sin(|{}^{\mathrm{light}}u^{\ddagger}|/2)}{|{}^{\mathrm{heavy}}u^{\ddagger}|/2 \,/\, \sin(|{}^{\mathrm{heavy}}u^{\ddagger}|/2)}, \qquad u^{\ddagger} = h\nu^{\ddagger}/k_{\mathrm{B}}T \quad (6)$$

Tunneling corrections are important in calculating heavy atom KIEs, particularly when the KIE is >1.01,[50] even when the contribution from tunneling is known to be small.[23] The match between frequencies generated by QUIVER from the Cartesian force constants and the scaled Gaussian 03/09 frequencies was checked routinely. They did not match in ONIOM models, for unknown reasons. The 3-^{14}C and 3,3-$^2H_2$ KIEs for **13-TS-oniom** were therefore calculated directly from isotopically substituted frequency calculations in Gaussian 03.

Because calculated KIEs are determined equally by the reactant and TS models, KIEs were calculated using matching pairs of reactant and TS molecules, i.e., with the same counterion and solvation (Tables S1−S3). The effects of different reactant models were tested for several TS models and were found to be modest (Table S1). Different models for solvation around C3 were tested. Reactant models were tested that had no solvation around C3 (e.g., **14-EP**), a carboxylic acid (e.g., **10-EP**), or water in place of hydronium ion (e.g., **16-EP**). Attempts to optimize reactant models containing hydronium ion were unsuccessful, as it was too reactive. The effects on the calculated 3-^{14}C KIEs were negligible, and they were modest for 3,3-$^2H_2$ KIEs.

dx.doi.org/10.1021/ja3043382 | J. Am. Chem. Soc. 2012, 134, 12947−12957

RESULTS

Solvent Deuterium KIE (SDKIE). SDKIEs of EPSP hydrolysis were determined noncompetitively from the ratio of reaction rates in H_2O and D_2O. The observed SDKIE, $SDKIE_{observed}$, was large and normal, 6.7 ± 0.3 in 50 mM glycine buffer at pL 2.0 at 52 °C. As noncompetitive KIEs reflect the rate-limiting step, this demonstrated that C3 protonation was rate-limiting.

Exchange Rate and First Irreversible Step. It was necessary to identify the first irreversible step for EPSP hydrolysis because competitive KIEs, where both isotopic labels are present in the same reaction, reflect the first irreversible step of a reaction (as well as any partially irreversible steps before the first fully irreversible step).[26,51,52] This was done by comparing the rate constant for EPSP hydrolysis (k_{hyd} = 1 × 10^{-4} s^{-1})[8] with solvent proton exchange into EPSP (k_{ex}), as measured by mass spectrometry. Solvent ^1H exchange into [3,3-$^2H_2$]EPSP, k_{ex}, was near the limit of detection and appeared negative in one experiment. The ratio k_{ex}/k_{hyd} was 0.01 ± 0.06, with the highest observed value being 0.04. Thus, C3 protonation was irreversible, and it was either the first irreversible step or occurred after the first irreversible step. Protonation of the vinyl ether group of α-methoxystyrene was also irreversible.[18]

Competitive KIEs. Competitive KIEs were measured for every atom in the carboxyvinyl part of EPSP using $^{32}P/^{33}P$ as a reporter label (Table 1, Scheme 3). The KIE on a remote ^{32}P label would be expected to be vanishingly small and was confirmed to be unity for AroA-catalyzed EPSP hydrolysis (see accompanying publication).[33] The 95% confidence intervals are reported for the experimental KIEs. The variability in the 1-^{14}C, 3,3-$^2H_2$, and 5′-^{18}O KIEs was larger than expected and larger than the corresponding KIEs for the AroA-catalyzed reaction. The reason for this is not clear, though a similar trend was observed previously for noncatalyzed versus enzymatic NAD^+ hydrolysis, possibly implicating the harsher nonenzymatic reaction conditions as a source of variability.[39,53]

Table 1. Experimental KIEs for EPSP Hydrolysis, Plus Calculated KIEs at 363 K for 7-TS-scrf

		calcd KIEs
isotopic label	exptl KIE[a,b]	7-TS-scrf
1-^{14}C	1.010 ± 0.007 (4)	1.004
2-^{14}C	1.003 ± 0.003 (3)	1.005
3-^{14}C	1.009 ± 0.005 (4)	1.011
5′-^{18}O	0.978 ± 0.009 (10)	0.997
1,1-$^{18}O_2$	1.001 ± 0.004 (5)	1.001
3,3-$^2H_2$	1.002 ± 0.010 (6)	1.040

[a]Error is the 95% confidence interval. Number of independent trials given in parentheses. [b]^{14}C KIEs were measured using a mixture of ^{14}C- and [^{32}P]EPSP. ^{32}P acted as a reporter on ^{12}C at the position of interest. ^{18}O and ^2H KIEs were measured by incorporating ^{33}P as a reporter radionuclide (e.g., [5′-^{18}O,^{33}P]EPSP) and were corrected for the extent of ^{18}O or ^2H enrichment (see Materials and Methods).

Scheme 3

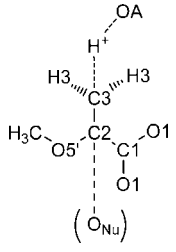

*Stepwise $A_H^{\ddagger}$*A_N or $A_H^{\ddagger}$ + A_N TS Structures.* Computational models and KIEs were calculated for a series of models based on enolpyruvyl methane (**1-EP**, Figures 1 and 2, Table 1).

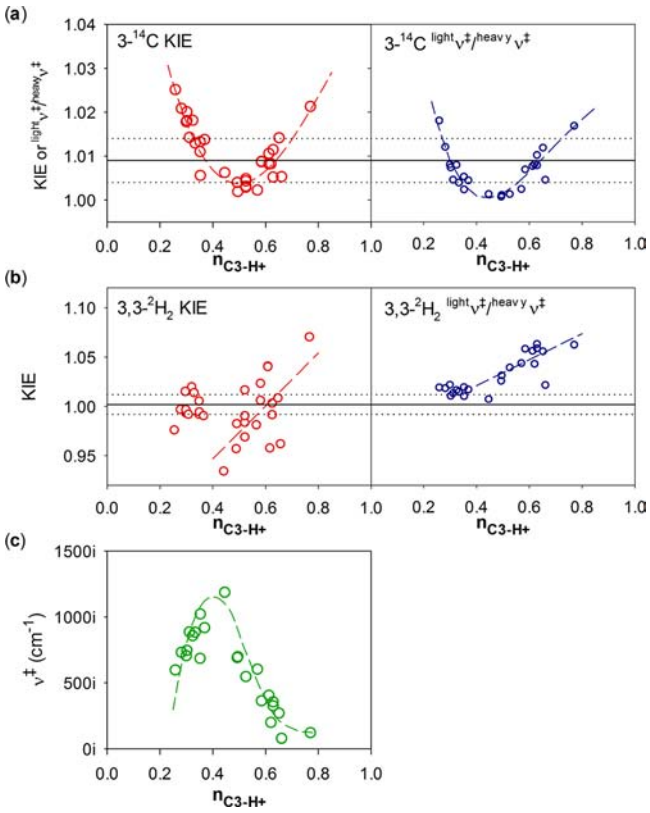

Figure 2. Calculated KIEs (left) and reaction coordinate contributions, $^{light}\nu^{\ddagger}/^{heavy}\nu^{\ddagger}$ (right) at 363 K for (a) 3-^{14}C and (b) 3,3-$^2H_2$, plus (c) the reaction coordinate frequencies ($\nu^{\ddagger}$). In parts a and b, the black horizontal lines represent the experimental KIE (solid line) and the 95% confidence interval (dotted lines). The dashed colored lines are intended only as visual aids. Other calculated KIEs are shown in Figure S1.

Models of the reactant, **1-EP**, transition state, **1-TS**, and oxacarbenium ion, **1-oxac**, were optimized at the B3PW91/6-31+G** level, as used previously.[51,54−56] The oxacarbenium ion **1-oxac** was computationally unstable; it formed an α-lactone, **29**, as previously observed for the oxacarbenium ion of sialic acid, **30**.[57] As a result, obtaining computational oxacarbenium ion and TS structures required one or more of the following: a counterion at the C1 carboxylate, protonation of the C1 carboxyl group, explicit water solvation, or continuum solvation (Figure 1). These all affected the calculated KIEs, particularly for the "bottom" half of the molecule: C1, O1, C2, and O5′ (see below). Models **24-EP-scrf** and **24-oxac-scrf** had calculated EIEs that were indistinguishable from those of the smaller models (Table S2), but **24-oxac-scrf** was prone to intramolecular deprotonation of C3 or hydroxyl addition to C2. These side reactions made optimization of larger oxacarbenium ion and TS models impractical.

Models **17-EP**, **14-EP**, **2-TS**, and **10-TS** were also optimized at the PBE0/aug-cc-pVDZ and MP2/aug-cc-pVDZ levels to

dx.doi.org/10.1021/ja3043382 | J. Am. Chem. Soc. 2012, 134, 12947−12957

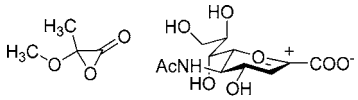

29 30

test the sensitivity of the models to the computational method. The structures and calculated KIEs from the three methods were very similar, and the results of the PBE0 and MP2 calculations were included in all analyses. When DFT and MP2 methods fail, it tends to be for different reasons (see ref 44), so the consistency of the results obtained here supports the reliability of the calculations.

Computational TS structures were solved with different combinations of acid catalyst, counterion, and solvating waters. They were performed in vacuo or with continuum solvation. Structure **7-TS-scrf**, as well as **10-TS** and **11-TS-scrf**, yielded calculated KIEs generally close to the experimental values, but not close enough to constitute prima facie evidence for its correctness. Instead, it was necessary to establish correlations between TS structures and calculated KIEs to validate this match. Computational TS structures were defined in terms of the Pauling bond order[58] of the C3−H^+ bond being formed, n_{C3-H+}, and ranged from 0.26 (**2-TS-scrf**) to 0.77 (**11-TS**). All the early calculated TS structures (n_{C3-H+} < 0.44) had hydronium as the acid catalyst, while all but one of the transition states with n_{C3-H+} > 0.49 had weaker, carboxylic acid catalysts. Any interaction of the C1 carboxylate with water, Li^+, guanidinium, or protonation decreased electron donation from the C1 carboxylate group to C2, destabilizing the cationic center at C2. This tended to cause a Hammond shift, resulting in later transition states.

The reaction coordinate was predominantly a linear transfer of H^+ from OA to C3 (Figure 3, Movie S1). There were varying amounts of coupling of other atoms to this motion in different TS structures, as reflected in the vibrational vectors (Figure 3) and in the reaction coordinate contributions ($^{light}\nu^{\ddagger}/^{heavy}\nu^{\ddagger}$) to individual calculated KIEs (Table S1). Reaction coordinate frequencies, $\nu^{\ddagger}$, were higher for balanced transition states and lower for early and late TS structures (Figure 2c), as expected.

There was a tight correlation between n_{C3-H+} and the bond order between H^+ and the acid catalyst, n_{H+-OA} (Figure 4). Σn_{H+} was essentially independent of model chemistry, as PBE0 and MP2 calculations yielded TS structures with Σn_{H+} values that were indistinguishable from B3PW91. Computational transition states of α-methoxystyrene protonation (**31**) had similar Σn_{H+} values of 0.82 ± 0.01 (calculated from bond lengths in Table 1 of ref 23).

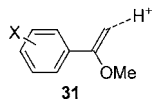

31

Concerted A_NA_H TS Structures. Computational TS structures were found for concerted addition of water across the C2−C3 double bond, using acetic acid (**25-TS**, **27-TS**) or formic acid (**26-TS**, **28-TS**) as the general acid catalyst. The structures were highly oxacarbenium ion-like, with significant C3−H^+ bond formation, n_{C3-H+} = 0.67 to 0.82, and very long C2−O_{Nu} bond lengths, with n_{C2-ONu} = 0.0001−0.04. This was expected, given our previous experimental results, which indicated that nucleophilic attack at C2 requires that C3 protonation be well advanced.[8]

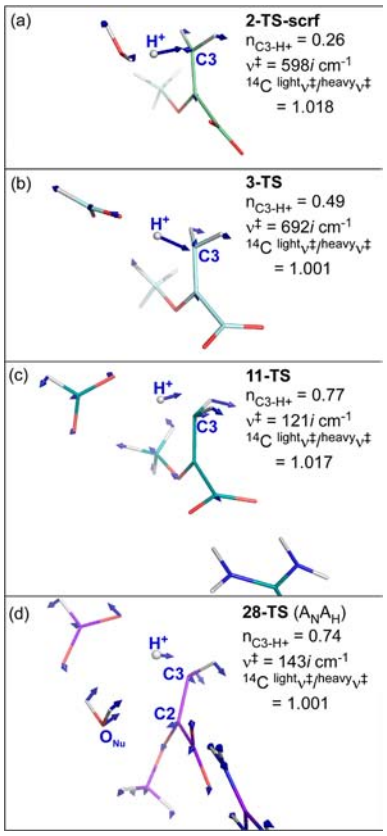

Figure 3. Reaction coordinate movements for $A^{\ddagger}_H$*A_N/$A^{\ddagger}_H$ + A_N transition states: (a) early (**2-TS-scrf**), (b) balanced (**3-TS**), and (c) late (**11-TS**) TS models. (d) A_NA_H **28-TS** model. The blue vectors illustrate the direction and magnitude of each atom's movement in the reaction coordinate (i.e., the normal coordinate with the imaginary frequency). The magnitudes of the vectors are comparable within each image but not between images. Animated reaction coordinates are available as Movies S1a, S1b, and S1c for the $A^{\ddagger}_H$*A_N/$A^{\ddagger}_H$ + A_N transition states.

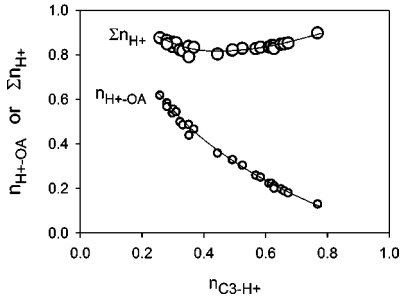

Figure 4. Total bond order to the transferring proton (Σn_{H+}) and H^+−OA bond order (n_{H+-OA}) as a function of C3−H^+ bond order (n_{C3-H+}) in computational TS structures.

The calculated 3-^{14}C and 3,3-$^2H_2$ KIEs for the A_NA_H transition states did not match the experimental values (Table S3). Specifically, the calculated 3-^{14}C KIEs were very small and often inverse, in the range 0.997−1.003. This was the result, in part, of the small reaction coordinate contribution ($^{light}\nu^{\ddagger}/^{heavy}\nu^{\ddagger}$ = 1.001−1.002), which was due, in turn, to the reaction coordinate being dominated by nucleophile motion rather than proton transfer (Figure 3d). The calculated 3,3-$^2H_2$ KIEs were in the range 0.90−0.94 (see Table S3). This was due to a large inverse structural contribution to the 3,3-$^2H_2$ KIE due

dx.doi.org/10.1021/ja3043382 | J. Am. Chem. Soc. 2012, 134, 12947−12957

to increased steric crowding and increased bond bending force constants as the sp^2-hybridized C3 is rehybridized toward sp^3.[59]

DISCUSSION

Acid-catalyzed hydrolysis of EPSP is the nonenzymatic analogue of the reaction catalyzed by AroA. AroA must protonate the nonbasic methylene carbon atom of PEP in the forward reaction, or EPSP in the reverse reaction, in order to form the tetrahedral intermediate. We showed previously that the rate enhancement of at least 5×10^8-fold associated with this protonation is sufficient on its own to account for AroA's observed overall rate enhancement of $\sim 10^9$-fold.[8] In the accompanying publication, we performed TS analysis on AroA-catalyzed EPSP hydrolysis.[33]

Possible Mechanisms. EPSP hydrolysis could begin with (i) C3 protonation in an $A_H{}^*A_N$ or $A_H + A_N$ mechanism,[60−62] (ii) concerted C3 protonation and nucleophilic attack at C2 in an A_NA_H mechanism, or (iii) unactivated nucleophilic attack at C2 ($A_N{}^*A_H$) (Figure 5). We showed previously that

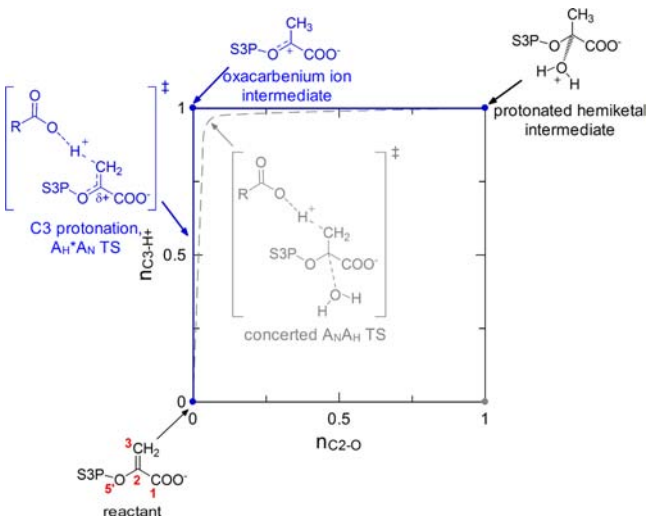

Figure 5. Reaction space for the first step(s) of EPSP hydrolysis. In this More O'Ferrall–Jencks plot,[64] the ordinate represents the bond order to the incoming proton (n_{C3-H+}), while the abscissa represents the bond order to the incoming water nucleophile (n_{C2-O}). If the reaction were stepwise $A_H{}^{\ddagger}{}^*A_N$, then the experimental KIEs would reflect oxacarbenium ion formation, whereas with a concerted A_HA_N mechanism they would reflect formation of the protonated hemiketal intermediate. From the protonated hemiketal intermediate, the ultimate products are S3P and pyruvate. The steps are the same in AroA-catalyzed EPSP hydrolysis.

unactivated nucleophilic attack on an enolpyruvyl group does not occur,[8] and the calculated EIEs for anion formation were not consistent with the experimental KIEs (Table S4), so the last possibility is eliminated. The first *irreversible* step could then be i or ii as above. Alternatively, it could be (iv) irreversible nucleophilic addition at C2 following reversible C3 protonation or (v) S3P departure from the tetrahedral intermediate (Figure 5). The fact that C3 protonation was irreversible eliminated the last two possibilities. The large SDKIE showed that C3 protonation was rate-limiting as well as irreversible.

The first irreversible step therefore involved C3 protonation, and the competitive KIEs therefore reflected either (i) C3 protonation to form the EPSP cation intermediate in an $A_H{}^{\ddagger}{}^*A_N$ or $A_H{}^{\ddagger} + A_N$ mechanism[60] or (ii) concerted water addition in an A_NA_H mechanism to form the protonated tetrahedral intermediate. The calculated 3-^{14}C and 3,3-$^2H_2$ KIEs for A_NA_H transition states were outside the range of the experimental values (Table S3), which therefore supports a stepwise $A_H{}^{\ddagger}{}^*A_N$ or $A_H{}^{\ddagger} + A_N$ mechanism.

The mechanism is $A_H{}^{\ddagger}{}^*A_N$ if the EPSP cation is too reactive to diffusionally equilibrate with solvent; otherwise, it is $A_H{}^{\ddagger} + A_N$. KIEs provide no information on this step, as it occurs after the first irreversible step, but there is some evidence that the EPSP cation is too short-lived to diffusionally equilibrate with solvent: (i) The product distribution in AroA tetrahedral intermediate breakdown was determined *after* the rate limiting step by P_i's protonation state in the EPSP cation·P_i ion pair complex, arguing that the complex was too reactive to diffusionally equilibrate with solvent.[11] (ii) The oxacarbenium ion of sialic acid (**30**) is too reactive to fully equilibrate with solvent.[62] Nevertheless, several oxacarbenium ions lacking an α-carboxyl group have sufficiently long lifetimes to potentially allow diffusional equilibration with solvent,[63] so the same is possible with the EPSP cation. Thus, the evidence favors an $A_H{}^{\ddagger}{}^*A_N$ mechanism, though $A_H{}^{\ddagger} + A_N$ is also possible.

The fact that C3 protonation was irreversible was consistent with most other enol ether protonations,[18,65,66] though partially reversible protonation has been observed.[67] This showed that the energetic barrier to proton transfer at a carbon atom, even a highly acidic one ($pK_a < -4$ for EPSP cation),[68] is greater than the almost barrierless nucleophilic addition to oxacarbenium ions.[65,69] In a previous study, nonenzymatic breakdown of the AroA THI proceeded through P_i departure to form an EPSP cation·P_i ion pair.[11] There was some EPSP formation, indicating EPSP cation deprotonation; however, that was in the context of the EPSP cation·P_i ion pair complex. Presumably P_i was acting as a general base catalyst and/or stabilizing the EPSP cation against nucleophilic attack, increasing its lifetime enough to make C3 deprotonation competitive.[11] In the current study, with no P_i present, there was no observable deprotonation of the EPSP cation.

KIE Interpretation. Solving a TS structure typically involves quantum mechanical optimization of reactant and TS models, then using vibrational frequencies to calculate KIEs. Vibrational frequencies from hybrid DFT methods generally accurately reflect the molecular structure,[49,70] and KIEs are a simple analytical function of vibrational frequencies;[25,48,71,72] therefore, KIEs accurately reflect the underlying reactant and TS structures (with the possible exception of primary KIEs in proton transfer; see below). Thus, when the calculated KIEs for a TS structure closely match the experimental values, this is considered to be the experimental transition state. It is generally possible to find a computational TS model with an excellent match to the experimental KIEs, particularly for heavy atoms labels,[25,32,50,72,73] though the errors on ^{2}H KIEs tend to be larger.[50] Conversely, when the calculated KIEs do not match the experimental values well, this is a sign that the computational models do not fully reflect reality, rather than there being a problem with the KIE calculation itself.

In the current study, structure **7-TS-scrf** provided a reasonable match to the experimental KIEs (as did **10-TS** and **11-TS-scrf**), but the calculated KIEs from many TS models were needed to establish structure-KIE relationships and interpret the experimental KIEs.

Computational modeling of primary hydron KIEs requires more advanced methods than employed in this study. For example, there were significant numerical contributions to the

dx.doi.org/10.1021/ja3043382 | J. Am. Chem. Soc. 2012, 134, 12947−12957

primary ^{2}H KIE from anharmonicity and tunneling effects in a computational study of **31** protonation, even though only a minor fraction of the reaction involved tunneling.[23] This was true even though the TS structures themselves were well modeled at B3LYP/6-31+G**, a similar level of theory to that used here. In addition, primary ^{2}H KIEs often do not generally distinguish well between competing TS models.[14,74] Thus, in the following discussion, the SDKIE is analyzed qualitatively while the other KIEs are analyzed computationally.

Solvent Deuterium KIE. $SDKIE_{observed}$ for EPSP hydrolysis was 6.7 ± 0.3. Large SDKIEs correlate with early transition states, and the observed SDKIE was larger than most literature SDKIEs for vinyl ether hydrolyses;[13,14,20,75] however, it is necessary to convert the observed SDKIE to the intrinsic value before comparing it with literature values. Factors affecting the SDKIE include the following: (i) an EIE on ionization of the EPSP C1 carboxyl, (ii) an EIE on ionization of the general acid catalyst, glycine, and (iii) the nature of the general acid catalyst.

The first two factors can be accounted for numerically:

$$SDKIE_{observed} = SDKIE_{intrinsic} \times EIE_{C1} \times EIE_{glycine} \quad (7)$$

The carboxylate form of the EPSP C1 carboxyl group is 2250-fold more reactive than the carboxylic acid,[8] so reaction through the carboxylate form will predominate even at pL 2.0. Because carboxyl group pK_a values increase in D_2O,[76] there will be a higher proportion of the carboxylate form in H_2O than D_2O, giving rise to EIE_{C1}. Given pK_a = 3.77 for EPSP C1[68] and assuming a typical value of ΔpK_a = 0.45[76] gives EIE_{C1} = 2.8,[77] this treatment is similar to the "preionization mechanism" proposed by Kresge et al.[68] Conversely, a larger fraction of the glycine catalyst will be in the reactive carboxyl form in D_2O than in H_2O. Given pK_a = 2.34 and ΔpK_a = 0.45 gives $EIE_{glycine}$ = 0.8. Incorporating the EIE_{C1} and $EIE_{glycine}$ values into eq 7 gives $SDKIE_{intrinsic}$ = 3.0. In comparison, the $SDKIE_{observed}$ for H_3O^+-catalyzed EPSP hydrolysis at pL 2 was 5.7.[68] Applying the same correction for EIE_{C1} gives $SDKIE_{intrinsic}$ = 2.1.

The third factor is the nature of the acid catalyst, for which there is no simple numerical conversion. L_3O^+-catalysis systematically gives lower SDKIEs than carboxylic acid catalysis, largely due to the inverse secondary KIE on the nontransferred L-O bonds in L_3O^+.[20,75] SDKIEs for L_3O^+-catalyzed vinyl ether hydrolyses range from 1.3 to 4.2.[13,14,20] SDKIEs for carboxylic acid-catalyzed reactions include 6.8 for formic acid-catalyzed ethyl vinyl ether hydrolysis, cf. 2.9 for L_3O^+-catalysis,[75] and 5.0 for acetic acid-catalyzed prostacylin hydrolysis, cf. 3.0 for L_3O^+-catalysis.[78] The $SDKIE_{intrinsic}$ of 3.0 for EPSP hydrolysis was lower than the other carboxylic acid-catalyzed SDKIEs, suggesting a later transition state. As carboxylic-acid catalyzed vinyl ether hydrolysis would be expected to be roughly balanced or slightly late, based on Brønsted α values (see Introduction), this suggests a similar or later transition state for EPSP hydrolysis, bearing in mind the previous caveats about the difficulty of quantitative interpretation of SDKIEs.

Quantum tunneling has been observed in other hydrogen (H^+, $H^\bullet$, H^-) transfer reactions,[79] but there was no evidence for quantum tunneling in α-methoxystyrene (**31**) protonation, based on the temperature dependence and the ratio of preexponential terms in an Arrhenius analysis, with A_H/A_D being unity,[18,22] or in other vinyl ether hydrolyses.[75] A computational study on the same molecules found small tunneling contributions for balanced transition states, which decreased for late transition states and was completely negligible for TS structures with bond orders for the forming C−H bond ≥0.65.[23]

3-^{14}C KIEs. The calculated 3-^{14}C and 3,3-$^2H_2$ KIEs varied systematically as a function of the extent of proton transfer, as reflected in the n_{C3-H+} value. Calculated KIEs were maximal for early and late TS structures and a minimum for balanced transition states, where $n_{C3-H+} \approx 0.5$ (Figure 2). The 3-^{14}C KIE correlated with the reaction coordinate contribution, $^{light}\nu^{\ddagger}/{}^{heavy}\nu^{\ddagger}$, while the "structural contribution", ZPE × EXC × VP, was essentially independent of n_{C3-H+}. The reaction coordinate contribution was in turn inversely correlated with the reaction coordinate frequency, $\nu^{\ddagger}$ (compare Figure 2a, c), with lower frequencies being correlated with larger $^{light}\nu^{\ddagger}/{}^{heavy}\nu^{\ddagger}$ values.

The source of this correlation becomes apparent when examining the normal mode corresponding to the imaginary frequencies (Figure 3). The earliest transition state was **2-TS-scrf**, with n_{C3-H+} = 0.26. The reaction coordinate consisted mostly of the in-flight proton (H^+) approaching C3. C3 moved slightly toward the H^+ and the H3s moved away as C3 rehybridized from sp^2 to sp^3 (Figure 3a, Movie S1a). In other words, movements of C3 and H^+ were coupled in the normal vibrational mode defining the reaction coordinate. This was typical of early TS structures. The coupling decreased in more balanced TS structures. **3-TS**, with n_{C3-H+} = 0.49, was typical of balanced TS structures. There was essentially no coupling of C3 with H^+ (Figure 3b, Movie S1b). In late TS structures (n_{C3-H+} > 0.58), with their lower imaginary frequencies, C3 motion once again became coupled with H^+, though C3 moved *away* from the in-flight proton. Because the H^+ vector was larger than C3′s, H^+ "caught up" to C3, and n_{C3-H+} increased as H^+ moved toward C3 in the reaction coordinate. This was typical of the late TS structures, with **11-TS** representing the extreme case, with n_{C3-H+} = 0.77 (Figure 3c, Movie S1c). The reason for C3 moving away from the in-flight proton was not clear, but it was a consistent feature of late TS structures. At the extremes of early and late TS structures, the reaction coordinate frequency was as low as 121*i* cm^{-1} (**11-TS**), and the reaction coordinate contribution to the 3-^{14}C KIEs was as high as $^{light}\nu^{\ddagger}/{}^{heavy}\nu^{\ddagger}$ = 1.018 (**2-TS-scrf**). In more balanced TS structures, $\nu^{\ddagger} \approx 1200i$ cm^{-1}, and the reaction coordinate contribution to the 3-^{14}C KIEs were as low as 1.001 (**2-TS**). Presumably in the balanced TS structures, the reaction coordinate frequency was too high for the heavy C3 atom to couple with H^+ through the weak C3−H^+ bond that was being formed. Coupling of C3 with H^+ motion in the early and late TS structures led to large reaction coordinate contributions to the calculated 3-^{14}C KIEs.

3,3-$^2H_2$KIE. The calculated 3,3-$^2H_2$ KIEs were relatively constant for early TS models, up to n_{C3-H+} = 0.37 (Figure 2b). These early TS models had reaction coordinates where C3 moved toward H^+ (Figure 3a). Beginning at n_{C3-H+} = 0.44, the reaction coordinate had little C3 motion toward H^+ (Figure 3b), and there was a roughly linear relationship between n_{C3-H+} and calculated 3,3-$^2H_2$ KIEs (Figure 2b). The reaction coordinate contributions increased in later transition states, reflecting coupling of the H3's motion with H^+, while the structural contribution was generally inverse, reflecting the loss of out-of-plane bending modes from the reactant's planar, sp^2-hybridized C3 atom, and increased constraints in bending modes as C3 was rehybridized toward sp^3.[59] The scatter in calculated values was relatively large (Figure 2b), consistent with previous observations that, even in cases where calculated heavy atom KIEs match the experimental values very well, there

was greater variation in calculated ^{2}H and ^{3}H KIEs.[50,55,56] The source of this variability is not known, but it could be due to contributions from anharmonicity, multidimensional tunneling, or variational TS effects.

Most of the calculated 3,3-$^{2}H_2$ KIEs for early TS models matched the experimental value, 1.002, relatively well, and though there was significant scatter in later TS models, the trend line matched the experimental value at n_{C3-H+} = 0.61. The calculated 3,3-$^{2}H_2$ KIE = 1.04 for **7-TS-scrf** (n_{C3-H+} = 0.61) was above the trend line, but given the greater reliability of calculated heavy atom KIEs, which matched the experimental values well, they were given more weight in choosing a TS model. The high 3,3-$^{2}H_2$ KIE for **7-TS-scrf** arose from a less inverse structural contribution, though the structure around H3 (e.g., n_{C3-H3}, bond angles) was not noticeably different from those of similar TS models (e.g., **10-TS**, n_{C3-H+} = 0.62, 3,3-$^{2}H_2$ KIE = 0.955, or **11-TS-scrf**, n_{C3-H+} = 0.65, 3,3-$^{2}H_2$ KIE = 1.008).

5′-^{18}O KIEs. Oxacarbenium ion-like TS structures will have inverse 5′-^{18}O KIEs, as the lone pair electrons of O5′ form a π-bond with C2. The experimental 5′-^{18}O KIE was inverse: 0.978 ± 0.009. The 95% confidence interval was large, even after 10 independent KIE measurements, but it was clearly inverse.

The oxacarbenium ion-like transition states in glycoside hydrolyses generally give inverse ring ^{18}O KIEs, as the cationic center at the anomeric carbon is stabilized by π-bonding from the ring oxygen. They are generally in the range of 0.98−0.99,[26,39,53,80] and in the cases where experimental and calculated KIEs have been compared, there has been a good match.[39,53] The most relevant comparison for EPSP hydrolysis is sialoside hydrolysis, where there is a carboxyl group adjacent to the cationic center (**30**). The ring ^{18}O KIE for hydrolysis was 0.975.[81] The ^{18}O KIE for EPSP hydrolysis would be expected to be broadly similar to those for glycoside hydrolysis, as the experimental value, 0.978, was.

The calculated ^{18}O KIEs were mostly inverse, ranging from 0.992 to 1.002 (Table S1). The sole normal KIE, 1.002, was due to an unusually large reaction coordinate contribution ($^{light}\nu^{\ddagger}/^{heavy}\nu^{\ddagger}$ = 1.005). The calculated EIEs for oxacarbenium ion formation, 0.986−0.996 (Table S2), were more inverse than the KIEs, as expected given that there is no reaction coordinate contribution in EIEs, and the oxacarbenium ion is fully developed. The less-inverse-than-expected IEs appear to arise from the fact that the calculated O5′−C2 bond order, $n_{O5'-C2}$, increased less than n_{C2-C3} decreased as the C2−C3 double bond became a single bond. The average increase in $n_{O5'-C2}$ was only 47% of the decrease in n_{C2-C3} (Figure S2), whereas in models of glycoside hydrolyses increases in bonding to the ring oxygen at least equal the loss of the glycoside bond.[39,53,55] In this respect, the computational model of EPSP hydrolysis did not fully match the experimental values.

Other KIEs. There was no discernible correlation between n_{C3-H+} and the other calculated ^{14}C KIEs; i.e., 1-^{14}C, 2-^{14}C (Figure S1). Given the reliable relationship between structure and calculated KIEs discussed above, this indicates that the structures of the "bottom" half of the models were determined largely by interactions with the general acid, counterions, solvating waters, or by continuum solvation, and they were only weakly affected by n_{C3-H+}. There were some correlations between, for example, the 1-^{14}C and 1,1-$^{18}O_2$ KIEs and the 1-^{14}C and 2-^{14}C KIEs, as these atoms were bonded together, but none between these KIEs and the 3-^{14}C or 3,3-$^{2}H_2$ KIEs (data not shown). There was a weak correlation between n_{C3-H+} and 1,1-$^{18}O_2$ KIEs (Figure S1). Calculated 1,1-$^{18}O_2$ KIEs increased at high n_{C3-H+} values due to the C2 cationic center becoming more electron withdrawing, which in turn increased n_{C1-C2} and decreased n_{C1-O1}. The effect was weak, with all but two of the calculated values falling within the confidence interval of the experimental 1,1-$^{18}O_2$ KIE. Even though there was no *systematic* correlation for these calculated KIEs, the match of **7-TS-scrf** KIEs with the experimental values was reasonable.

EXPERIMENTAL TS STRUCTURE

The best overall match of calculated to experimental KIEs was for model **7-TS-scrf**, a moderately late transition state with n_{C3-H+} = 0.61. The calculated 3-^{14}C KIEs best matched the experimental value of 1.009 ± 0.005 for moderately early and late TS structures (n_{C3-H+} = 0.37 and 0.64, respectively), with the calculated KIEs for balanced transition states dropping below the experimental KIE's 95% confidence interval. The best matches of calculated to the experimental 3,3-$^{2}H_2$ KIE of 1.002 ± 0.010 were for very early TS models, and for $n_{C3-H+} \approx$ 0.6. Other evidence supports a moderately late transition state. The $SDKIE_{intrinsic}$ value was lower than the maximum literature values, indicating a slightly later transition state. The experimental 5′-^{18}O KIE was inverse and large, 0.978 ± 0.009, similar to the value of 0.975 for a sialyl glycoside hydrolysis reaction, for which the KIEs indicated a highly oxacarbenium ion-like transition state.[81] The general acid catalyst in **7-TS-scrf** was a carboxylic acid, consistent with the fact that, under the experimental conditions in this study, the general acid catalyst was acetic acid rather than H_3O^+.[18,68] All computational models with early transition states (n_{C3-H+} < 0.44) had hydronium ion as the acid catalyst, while all but one of the transition states with n_{C3-H+} > 0.49 had a carboxylic acid catalyst, again supporting a moderately late transition state.

This conclusion is supported by the calculated KIEs for **7-TS-scrf**. While there was no systematic relationship between n_{C3-H+} and the calculated 1-^{14}C and 2-^{14}C KIEs, there was a good match between the calculated ^{14}C KIEs for **7-TS-scrf** (n_{C3-H+} = 0.61) and the experimental KIEs (Table 1), except that the calculated 5′-^{18}O KIE was less inverse than expected, as discussed above. The calculated 1-^{14}C KIE was within experimental error of the experimental value. The trend line for calculated 3,3-$^{2}H_2$ KIEs matched the experimental value at n_{C3-H+} = 0.61. The calculated KIEs for **10-TS** (n_{C3-H+} = 0.62) and **11-TS-scrf** (n_{C3-H+} = 0.65) were also in reasonable agreement with the experimental values. Together these calculated KIEs demonstrate a moderately late experimental TS structure, with $n_{C3-H+} \approx$ 0.6.

CONCLUSIONS

TS analysis of acid-catalyzed EPSP hydrolysis demonstrated that it had a transition state with significant oxacarbenium ion character and a stepwise $A_H^{\ddagger}*A_N$ mechanism. That is, the reaction proceeded through rate-limiting and irreversible protonation at C3 to form an oxacarbenium ion intermediate. The rate-limiting nature of proton transfer was demonstrated by the large solvent deuterium KIE, while the lack of solvent hydron incorporation into EPSP showed that C3 protonation was irreversible. The primary 3-^{14}C KIE correlated with the extent of proton transfer at the transition state, as did the secondary 3,3-$^{2}H_2$ KIEs to a lesser extent. The 3-^{14}C KIE was dominated by the reaction coordinate contribution,

dx.doi.org/10.1021/ja3043382 | J. Am. Chem. Soc. 2012, 134, 12947−12957

$^{light}\nu^{\ddagger}/^{heavy}\nu^{\ddagger}$, which reflected coupling of C3 with the transferring proton, H^+, in the reaction coordinate. The experimental KIEs indicated a slightly late transition state, with a C3−H^+ bond order, n_{C3-H+} ≈0.6. The inverse experimental 5′-^{18}O KIE supported an oxacarbenium ion-like transition state. The calculated KIEs in the "bottom" half of the model compounds, i.e., 1-^{14}C, 2-^{14}C, and 1,1-$^{18}O_2$, were dominated by interactions with the counterions and solvation in the computational models, and they did not correlate with the extent of proton transfer, n_{C3-H+}. Nonetheless, there was a good match of the calculated KIEs for model **7-TS-scrf** with the experimental KIEs. This transition state reveals the intrinsic reactivity of EPSP, and comparison with the AroA-catalyzed reaction illustrates how the enzyme interacts with this reactivity to catalyze its reaction.[33]

■ ASSOCIATED CONTENT

Ⓢ Supporting Information

Complete citation for ref 42, calculated KIEs, plot of $n_{C2-OS'}$ vs n_{C2-C3}, reaction coordinate contributions, calculated EIEs, and Cartesian coordinates for computational models. This material is available free of charge via the Internet at http://pubs.acs.org.

Ⓦ Web-Enhanced Feature

Animated reaction coordinates for the $A^{\ddagger}_{H}$*A_N/$A^{\ddagger}_{H}$ + A_N transition states.

■ AUTHOR INFORMATION

Corresponding Author

berti@mcmaster.ca

Notes

The authors declare no competing financial interest.

[§]née Clark.

■ ACKNOWLEDGMENTS

We thank Fuzhong Zhang for developing the [1,1-$^{18}O_2$]PEP synthesis, Paul Chindemi for AroA production, and Prof. David Jakeman (Dalhousie University) for the plasmid to overexpress phosphoenolpyruvate synthetase. We also thank Prof. Paul Ayers (McMaster) for many helpful discussions. This work was supported by Canadian Institutes of Health Research Operating Grant MOP-64422.

■ REFERENCES

(1) Richard, J. P.; Amyes, T. L.; Williams, K. B. *Pure Appl. Chem.* **1998**, *70*, 2007−2014.

(2) Wendt, K. U.; Schulz, G. E.; Corey, E. J.; Liu, D. R. *Angew. Chem., Int. Ed. Engl.* **2000**, *39*, 2812−2833.

(3) Gerlt, J. A.; Babbitt, P. C. *Annu. Rev. Biochem.* **2001**, *70*, 209−246.

(4) Tanner, M. E. *Acc. Chem. Res.* **2002**, *35*, 237−246.

(5) Abbreviations: $A_H^{\ddagger}$*A_N, a stepwise addition mechanism with protonation being the first, rate-limiting step; A_NA_H, concerted addition mechanism; AroA, EPSP synthase; AroK, shikimate kinase; CPCM, conductor-like polarizable continuum model; cpm, counts per min; EIE, equilibrium isotope effect; EPSP, 5-enolpyruvylshikimate 3-phosphate; ESI-MS, electrospray ionization mass spectra; EXC, excited state contribution to KIEs; KIE, kinetic isotope effect; MurA, UDP-*N*-acetylglucosamine enolpyruvyl transferase; PEP, phosphoenolpyruvate; P_i, inorganic phosphate; PIE, product isotope effect; ppsA, phosphoenolpyruvate synthetase; S3P, shikimate 3-phosphate; SCRF, self-consistent reaction field; SDKIE, solvent deuterium kinetic isotope effect; TBAS, tetrabutylammonium sulfate; THI, tetrahedral intermediate; TS, transition state; VP, vibrational product; ZPE, zero point energy contribution to KIEs.

(6) Anderson, K. S.; Johnson, K. A. *Chem. Rev.* **1990**, *90*, 1131−1149. Steinrucken, H. C.; Amrhein, N. *Biochem. Biophys. Res. Commun.* **1980**, *94*, 1207−1212.

(7) Berti, P. J.; Chindemi, P. *Biochemistry* **2009**, *48*, 3699−3707.

(8) Clark, M. E.; Berti, P. J. *Biochemistry* **2007**, *46*, 1933−1940.

(9) Zhang, F.; Berti, P. J. *Biochemistry* **2006**, *45*, 6027−6037.

(10) Mizyed, S.; Wright, J. E. I.; Byczynski, B.; Berti, P. J. *Biochemistry* **2003**, *42*, 6986−6995.

(11) Byczynski, B.; Mizyed, S.; Berti, P. J. *J. Am. Chem. Soc.* **2003**, *125*, 12541−12550.

(12) Hendlin, D.; Stapley, E. O.; Jackson, M.; Wallick, H.; Miller, A. K.; Wolf, F. J.; Miller, T. W.; Chaiet, L.; Kahan, F. M.; Foltz, E. L.; Woodruff, H. B.; Mata, J. M.; Hernandez, S.; Mochales, S. *Science* **1969**, *166*, 122−123. Schonbrunn, E.; Sack, S.; Eschenburg, S.; Perrakis, A.; Krekel, F.; Amrhein, N.; Mandelkow, E. *Structure* **1996**, *4*, 1065−1075. Gunetileke, K. G.; Anwar, R. A. *J. Biol. Chem.* **1968**, *243*, 5770−5778. Jackson, S. G.; Zhang, F.; Chindemi, P.; Junop, M. S.; Berti, P. J. *Biochemistry* **2009**, *48*, 11715−11723.

(13) Kresge, A. J. *Acc. Chem. Res.* **1987**, *20*, 364−370.

(14) Kresge, A. J.; Sagatys, D. S.; Chen, H. L. *J. Am. Chem. Soc.* **1977**, *99*, 7228−7233.

(15) Bell, R. P., *The Proton in Chemistry*, 2nd ed.; Cornell University Press: Ithaca, NY, 1973.

(16) Kresge, A. J.; Chiang, Y. *J. Am. Chem. Soc.* **1973**, *95*, 803−806.

(17) Chwang, W. K.; Eliason, R.; Kresge, A. J. *J. Am. Chem. Soc.* **1977**, *99*, 805−808.

(18) Tsang, W. Y.; Richard, J. P. *J. Am. Chem. Soc.* **2009**, *131*, 13952−13962.

(19) Kreevoy, M. M.; Eliason, R. *J. Phys. Chem.* **1968**, *72*, 1313−1316.

(20) Chiang, Y.; Cho, M. J.; Euser, B. A.; Kresge, A. J. *J. Am. Chem. Soc.* **1986**, *108*, 4192−4196.

(21) Kresge, A. J.; Chen, H.-L.; Chiang, Y.; Murrill, E.; Payne, M. A.; Sagatys, D. S. *J. Am. Chem. Soc.* **1971**, *93*, 413−423.

(22) Tsang, W. Y.; Richard, J. P. *J. Am. Chem. Soc.* **2007**, *129*, 10330−10331.

(23) Wong, K. Y.; Richard, J. P.; Gao, J. L. *J. Am. Chem. Soc.* **2009**, *131*, 13963−13971.

(24) Schramm, V. L. *Acc. Chem. Res.* **2003**, *36*, 588−596.

(25) Berti, P. J.; McCann, J. A. B. *Chem. Rev.* **2006**, *106*, 506−555.

(26) Berti, P. J.; Tanaka, K. S. E. *Adv. Phys. Org. Chem.* **2002**, *37*, 239−314.

(27) Buddenbaum, W. E.; Yankwich, P. E. *J. Phys. Chem.* **1967**, *71*, 3136−3143.

(28) Berti, P. J. *Methods Enzymol.* **1999**, *308*, 355−397.

(29) VP is the vibrational product derived from the Teller-Redlich rule: VP = $vp_{TS}/vp_{reactant,}$ $vp = \prod_{i}^{x}(^{light}\nu/^{heavy}\nu)$, where x = 3N-7 (TS) or 3N-6 (reactant), and N = the number of atoms.[30] MMI, the contribution from mass and moments of inertia, is given by MMI = $^{light}\nu^{\ddagger}/^{heavy}\nu^{\ddagger}$ × VP. Wilson, E. B., Jr.; Decius, J. C.; Cross, P. C., *Molecular Vibrations: The Theory of Infrared and Raman Vibrational Spectroscopy*; McGraw-Hill: New York, 1955.

(30) Suhnel, J.; Schowen, R. L. In *Enzyme mechanism from isotope effects*, Cook, P. F., Ed.; CRC Press, Inc.: Boca Raton, FL, 1991; pp 3−35.

(31) Bell, R. P. *Trans. Faraday Soc* **1959**, *55*, 1−4.

(32) Hirschi, J. S.; Takeya, T.; Hang, C.; Singleton, D. A. *J. Am. Chem. Soc.* **2009**, *131*, 2397−2403.

(33) Lou, M.; Burger, S. K.; Gilpin, M. E.; Gawuga, V.; Capretta, A.; Berti, P. J. *J. Am. Chem. Soc.* **2012**, DOI: 10.1021/ja304339h.

(34) Jakeman, D. L.; Evans, J. N. S. *Bioorg. Chem.* **1998**, *26*, 245−253.

(35) Bradford, M. M. *Anal. Biochem.* **1976**, *72*, 248−254.

(36) Oliveira, J. S.; Pinto, C. A.; Basso, L. A.; Santos, D. S. *Protein Expr. Purif.* **2001**, *22*, 430−435.

(37) Wright, S. K.; DeClue, M. S.; Mandal, A.; Lee, L.; Wiest, O.; Cleland, W. W.; Hilvert, D. *J. Am. Chem. Soc.* **2005**, *127*, 12957−12964.

(38) Unrau, P. J.; Bartel, D. P. *Proc. Natl. Acad. Sci. U.S.A.* **2003**, *100*, 15393−15397. Parkin, D. W. In *Enzyme mechanism from isotope effects*, Cook, P. F., Ed.; CRC Press, Inc.: Boca Raton, FL, 1991; pp 269−290.
(39) Berti, P. J.; Blanke, S. R.; Schramm, V. L. *J. Am. Chem. Soc.* **1997**, *119*, 12079−12088.
(40) Becke, A. D. *Phys. Rev. A* **1988**, *38*, 3098−3100.
(41) Perdew, J. P.; Wang, Y. *Phys. Rev. B* **1992**, *45*, 13244.
(42) Frisch, M. J. et al. Gaussian 09, Gaussian, Inc.: Wallingford, CT, 2009.
(43) Cossi, M.; Rega, N.; Scalmani, G.; Barone, V. *J. Comput. Chem.* **2003**, *24*, 669−681. Barone, V.; Cossi, M. *J. Phys. Chem. A* **1998**, *102*, 1995−2001.
(44) Loncke, P. G.; Berti, P. J. *J. Am. Chem. Soc.* **2006**, *128*, 6132−6140.
(45) Dapprich, S.; Komaromi, I.; Byun, K. S.; Morokuma, K.; Frisch, M. J. *THEOCHEM* **1999**, *461*, 1−21.
(46) Peng, C. Y.; Schlegel, H. B. *Israel J. Chem.* **1993**, *33*, 449−454.
(47) Burger, S. K.; Ayers, P. W. *J. Chem. Phys.* **2010**, *132*, 234110.
(48) Saunders, M.; Laidig, K. E.; Wolfsberg, M. *J. Am. Chem. Soc.* **1989**, *111*, 8989−8994.
(49) Wong, M. W. *Chem. Phys. Lett.* **1996**, *256*, 391−399.
(50) Meyer, M. P.; DelMonte, A. J.; Singleton, D. A. *J. Am. Chem. Soc.* **1999**, *121*, 10865−10874.
(51) Chen, X.-Y.; Berti, P. J.; Schramm, V. L. *J. Am. Chem. Soc.* **2000**, *122*, 6527−6534.
(52) Fersht, A. R., *Enzyme structure and mechanism*, 2nd ed.; W. H. Freeman and Co.: New York, 1985.
(53) Berti, P. J.; Schramm, V. L. *J. Am. Chem. Soc.* **1997**, *119*, 12069−12078.
(54) Lee, J. K.; Bain, A. D.; Berti, P. J. *J. Am. Chem. Soc.* **2004**, *126*, 3769−3776. Chen, X.-Y.; Berti, P. J.; Schramm, V. L. *J. Am. Chem. Soc.* **2000**, *122*, 1609−1617.
(55) McCann, J. A. B.; Berti, P. J. *J. Am. Chem. Soc.* **2007**, *129*, 7055−7064.
(56) McCann, J. A. B.; Berti, P. J. *J. Am. Chem. Soc.* **2008**, *130*, 5789−5797.
(57) Horenstein, B. A. *J. Am. Chem. Soc.* **1997**, *119*, 1101−1107.
(58) Pauling bond order: $n_{ij} = \exp(r_1 - r_{ij})/0.3$, where r_{ij} is the distance between atoms i and j and r_1 is the single bond length between i and j.
(59) Matsson, O.; Westaway, K. C. *Adv. Phys. Org. Chem.* **1998**, *31*, 143−248. Poirier, R. A.; Wang, Y.; Westaway, K. C. *J. Am. Chem. Soc.* **1994**, *116*, 2526−2533.
(60) In IUPAC nomenclature, proton addition is an A_H step, and nucleophile addition is A_N.[62] An A_H*A_N mechanism is stepwise, with a discrete cationic intermediate that is too short-lived to diffusionally equilibrate with solvent. If the intermediate is sufficiently long-lived to diffusionally equilibrate with solvent, the mechanism would be $A_H + A_N$. Concerted addition of a nucleophile and a proton would be an A_NA_H mechanism. The rate-limiting step is indicated by the ‡ symbol.
(61) Guthrie, R. D.; Jencks, W. P. *Acc. Chem. Res.* **1989**, *22*, 343−349; Commission on Physical Organic Chemistry *Pure Appl. Chem.* **1989**, *61*, 23−56.
(62) Horenstein, B. A.; Bruner, M. *J. Am. Chem. Soc.* **1998**, *120*, 1357−1362.
(63) Amyes, T. L.; Jencks, W. P. *J. Am. Chem. Soc.* **1989**, *111*, 7888−7900.
(64) Jencks, W. P. *Chem. Rev.* **1985**, *85*, 511−527.
(65) Richard, J. P.; Williams, K. B.; Amyes, T. L. *J. Am. Chem. Soc.* **1999**, *121*, 8403−8404.
(66) Richard, J. P.; Jencks, W. P. *J. Am. Chem. Soc.* **1984**, *106*, 1373−1383.
(67) Richard, J. P.; Lin, S. S.; Buccigross, J. M.; Amyes, T. L. *J. Am. Chem. Soc.* **1996**, *118*, 12603−12613. Richard, J. P.; Amyes, T. L.; Lin, S. S.; O'Donoghue, A. C.; Toteva, M. M.; Tsuji, Y.; Williams, K. B. *Adv. Phys. Org. Chem.* **2000**, *35*, 67−115.
(68) Kresge, A. J.; Leibovitch, M.; Sikorski, J. A. *J. Am. Chem. Soc.* **1992**, *114*, 2618−2622.
(69) Richard, J. P. *Tetrahedron* **1995**, *51*, 1535−1573.
(70) Glad, S. S.; Jensen, F. *J. Phys. Chem.* **1996**, *100*, 16892−16898. Scott, A. P.; Radom, L. *J. Phys. Chem.* **1996**, *100*, 16502−16513.
(71) Bigeleisen, J.; Goeppert Mayer, M. *J. Chem. Phys.* **1947**, *15*, 261−267. Bigeleisen, J.; Wolfsberg, M. *Adv. Chem. Phys.* **1958**, *1*, 15−76.
(72) Schramm, V. L. *J. Biol. Chem.* **2007**, *282*, 28297−28300.
(73) Singleton, D. A.; Thomas, A. A. *J. Am. Chem. Soc.* **1995**, *117*, 9357−9358. Hirschi, J.; Singleton, D. A. *J. Am. Chem. Soc.* **2005**, *127*, 3294−3295.
(74) Nielsen, P. A.; Glad, S. S.; Jensen, F. *J. Am. Chem. Soc.* **1996**, *118*, 10577−10583. Glad, S. S.; Jensen, F. *J. Org. Chem.* **1997**, *62*, 253−260.
(75) Kresge, A. J.; Chiang, Y. *J. Chem. Soc., B* **1967**, 58−61.
(76) Bell, R. P.; Kuhn, A. T. *Trans. Faraday Soc* **1963**, *59*, 1789−1793.
(77) At pL 2, the fraction of EPSP C1 in the reactive carboxylate forms will be 0.017 in H_2O, and 0.0060 in D_2O. For the glycine general acid catalyst, the fraction of glycine in the reactive carboxyl form will be 0.69 in H_2O, and 0.86 in D_2O. Assuming ΔpK_a values of 0.40 to 0.55 gives estimated values of $SDKIE_{intrinsic}$ of 3.3 to 2.5, respectively.
(78) A separate SDKIE = 1.33 was measured for the intramolecularly general acid catalyzed reaction involving the carboxylate moiety of prostacyclin.[20]
(79) Kohen, A.; Klinman, J. P. *Chem. Biol.* **1999**, *6*, R191−R198.
(80) Indurugalla, D.; Bennet, A. J. *J. Am. Chem. Soc.* **2001**, *123*, 10889−10898.
(81) Chan, J.; Lewis, A. R.; Gilbert, M.; Karwaski, M. F.; Bennet, A. J. *Nat. Chem. Biol.* **2010**, *6*, 405−407.